Available online at www.sciencedirect.com
SCIENCE DIRECT®
ELSEVIER
Chemometrics and Intelligent Laboratory Systems 65 (2003) 159–178
Chemometrics and intelligent laboratory systems
www.elsevier.com/locate/chemometrics

Process monitoring using causal map and multivariate statistics: fault detection and identification

Leo H. Chiang, Richard D. Braatz*

Large Scale Systems Research Laboratory, Department of Chemical Engineering, University of Illinois at Urbana-Champaign, 600 South Mathews Avenue, Box C-3 Urbana, IL 61801-3792, USA

Received 1 August 2001; received in revised form 13 April 2002; accepted 19 June 2002

Abstract

Data-driven techniques based on multivariate statistics (such as principal component analysis (PCA) and partial least squares (PLS)) have been applied widely to chemical processes and their effectiveness for fault detection is well recognized. There is an inherent limitation on the ability for purely data-driven techniques to identify and diagnose faults, especially when the abnormal situations are associated with unknown faults or multiple faults. The modified distance (DI) and modified causal dependency (CD) are proposed to incorporate the causal map with data-driven approach to improve the proficiency for identifying and diagnosing faults. The DI is based on the Kullback–Leibner information distance (KLID), the mean of the measured variables, and the range of the measured variable. The DI is used to measure the similarity of the measured variable between the current operating conditions and the historical operating conditions. When the DI is larger than the predefined threshold, the variable is identified as abnormal. The CD, derived based on the multivariate T^2 statistic, is used to measure the causal dependency of two variables. When CD is larger than the predefined threshold, the causal dependency of the two variables is broken. The proposed method requires a causal map and historical data associated with the normal operating conditions. A causal map containing the causal relationship between all of the measured variables can be derived based on knowledge from a plant engineer and the sample covariance matrix from the normal data. The DI/CD algorithm outperformed the purely data-driven techniques such as PCA for detecting and identifying known, unknown, and multiple faults using the data sets from the Tennessee Eastman process (TEP).

Keywords: Fault detection; Fault identification; Process monitoring; Chemometrics methods; Causal map; Multivariate statistics

1. Introduction

Multivariate statistical methods such as principal component analysis (PCA) and partial least square (PLS) have been applied widely in chemical industries for process monitoring [1–8]. An advantage of multivariate statistical methods is that they are completely data-based—no sophisticated training is required for an engineer to apply the techniques. Therefore, multivariate statistics are especially well-suited for large-scale industrial processes. The main disadvantage of the purely data-driven techniques is that there is an inherent limitation on their ability to effectively identify and diagnose faults, especially when the abnormal

* Corresponding author. Tel.: +1-217-333-5073; fax: +1-217-333-5052.
E-mail address: braatz@uiuc.edu (R.D. Braatz).

0169-7439/02/$ - see front matter © 2002 Elsevier Science B.V. All rights reserved.
doi:10.1016/S0169-7439(02)00140-5

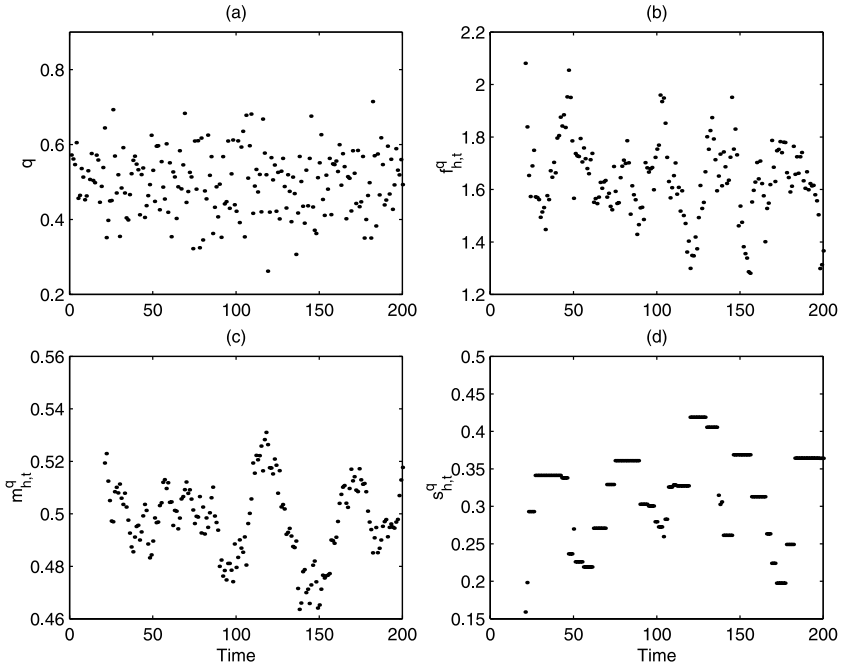

Fig. 1. Example 1: (a) The normalized plot, (b) the KLID between the distribution and the flat distribution, (c) the mean, and (d) the range for variable q under normal operating conditions.

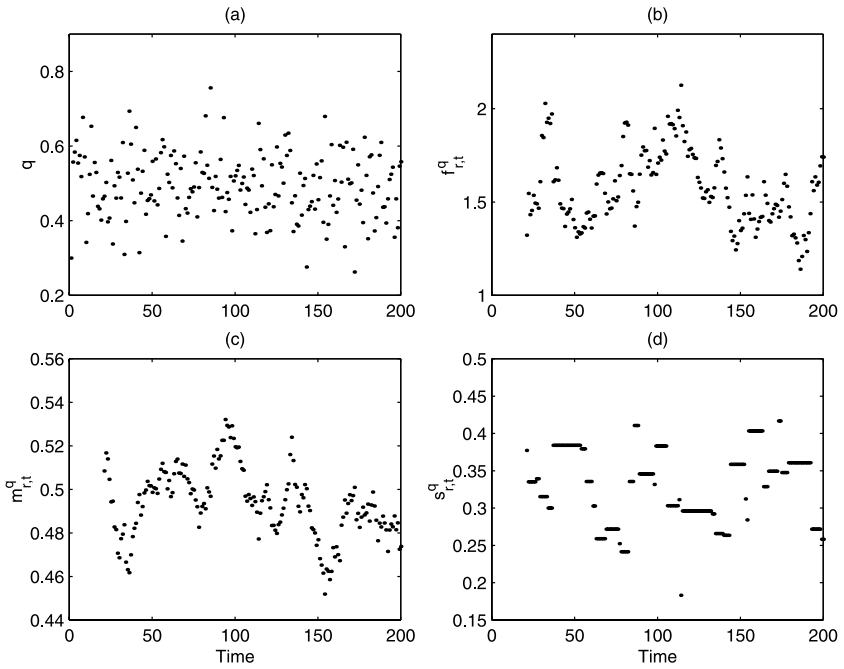

Fig. 2. Example 2: (a) The normalized plot, (b) the KLID between the distribution and the flat distribution, (c) the mean, and (d) the range for variable q under normal operating conditions.

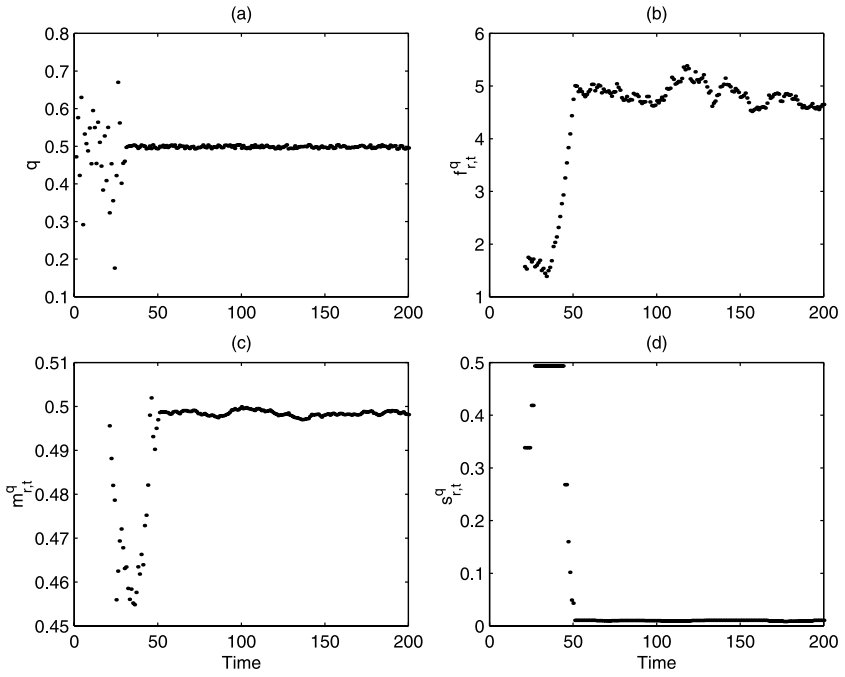

Fig. 3. Example 3: (a) The normalized plot, (b) the KLID between the distribution and the flat distribution, (c) the mean, and (d) the range for variable q under faulty conditions.

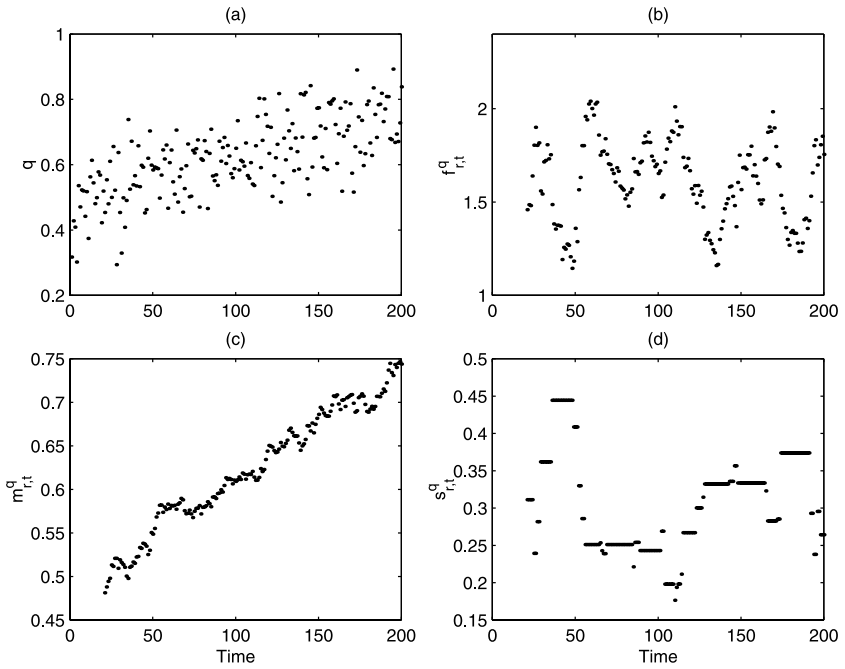

Fig. 4. Example 4: (a) The normalized plot, (b) the KLID between the distribution and the flat distribution, (c) the mean, and (d) the range for variable q under faulty conditions.

situations are associated with unknown faults or multiple faults. Knowledge-based approaches such as the signed directed graph (SDG) [9–12], fault tree analysis [13–15], and expert systems [16,17] have been proposed to address these issues. These techniques are based on qualitative models, which can be obtained through causal modeling of the system, expert knowledge, a detailed description of the system, or fault-symptom examples.

The SDG, fault tree analysis, and expert systems can improve fault diagnosis, but the main limitation to applying these methods for large-scale systems is the requirement of time-intensive collection of highly detailed information for the system. To improve the proficiency of data-driven techniques for fault identification and diagnosis, a less time-intensive method which incorporates causal analysis and data-driven techniques is proposed in this paper. Section 2 describes the entropy-based measures based on the SELMON system, which provides some background for understanding the proposed algorithm. This is followed by a description of the proposed algorithm. Section 3 evaluates the proposed method using data sets from a chemical plant simulator. Section 4 summarizes the conclusions.

2. Methods

2.1. Entropy-based measures

The SELective MONitoring (SELMON) system was developed by Doyle et al. [18–20] in the artificial intelligence research group at the Jet Propulsion Laboratory. SELMON was designed to improve upon the performance of traditional monitoring systems by incorporating multiple measures to detect faults. SELMON detects changes in the frequency distributions

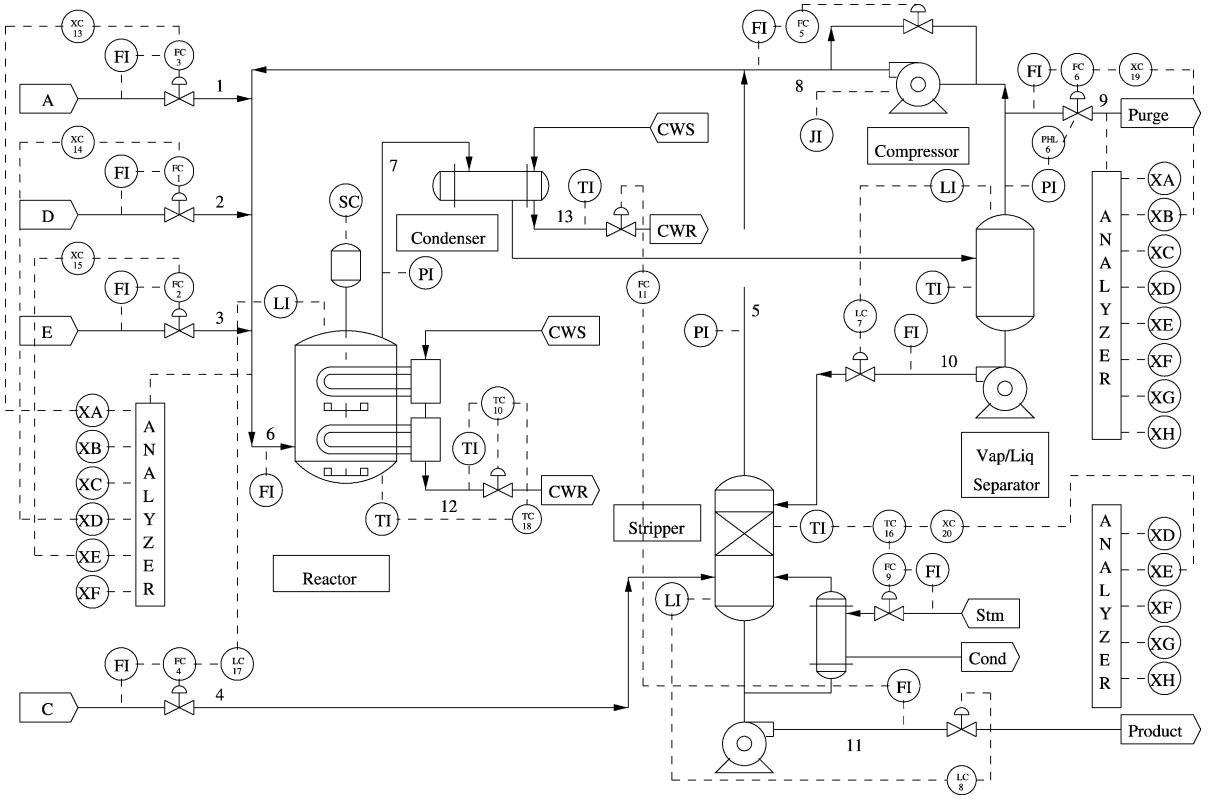

Fig. 5. A diagram of the Tennessee Eastman process simulator.

of sensor readings over time; it also detects changes in relationships among sensor readings. The two entropy-based measures, which can be extended for fault diagnosis, are discussed here.

The entropy-based measures are the *distance* and *causal distance*. Both measures are based on the frequency distributions of the sensor measurements. When a fault occurs, even if the observations or the deviation measures are within their normal limits, the frequency distribution of an observation variable or the relationship between the frequency distributions of two variables can change significantly. The distance and causal distance are designed for identifying these broken sensors and causal dependencies, respectively. The proficiency for detecting and identifying faults can potentially increase by integrating a causal map with the data-driven approach.

The main advantage of the distance and causal distance is that they are sensitive to faults associated with changes in the distributions of the measured variables. In situations where there are temporary shifts of the data away from the mean, or changes in variability of the measured variables around the mean, the distance and causal distance can produce a lower missed detection rate (type-II error) as compared to multivariate statistics (such as PCA) [21].

However, a weakness of the distance and causal distance is their strong dependence on the number of bins and the size of each bin. The main disadvantage is that collecting the data into different bins to define the distribution loses resolution. Also, several distinct distributions can result in the same measures. As such, important information can be lost which often leads to high false alarm rate (type-I error), especially for large-scale systems [22].

2.2. Incorporating the causal map with the data-driven approach

To take advantage of the entropy-based measures and to avoid the disadvantage associated with using bins, an algorithm based on the *modified distance* (DI) and the *causal dependence* (CD) is proposed. The DI is used to identify broken sensors, while the CD is used to identify broken causal dependencies.

The DI is derived from the Kullback–Leibner information distance (KLID), the mean of the measured variables, and the range of the measured variables. The continuous-time KLID [23] is defined as:

$$I(p*,\hat{p}) = \int p*(x)\ln\frac{p*(x)}{\hat{p}(x)}\mathrm{d}x. \quad (1)$$

where $p*(x)$ and $\hat{p}(x)$ are the distributions of the two sensors under examination, and the random variable x has been normalized by dividing the difference between its maximum and minimum values so that $0 \le x \le 1$.

To illustrate the concept of the modified distance, six examples will be shown. Examples 1 and 2 are associated with the normal operating conditions, while the rest are associated with faulty conditions. The data from Example 1 are treated as the training set, while

Table 1
Process faults for the Tennessee Eastman process simulator

Variable	Description	Type
IDV(1)	A/C Feed Ratio, B Composition Constant (Stream 4)	Step
IDV(2)	B Composition, A/C Ratio Constant (Stream 4)	Step
IDV(3)	D Feed Temperature (Stream 2)	Step
IDV(4)	Reactor Cooling Water Inlet Temperature	Step
IDV(5)	Condenser Cooling Water Inlet Temperature	Step
IDV(6)	A Feed Loss (Stream 1)	Step
IDV(7)	C Header Pressure Loss–Reduced Availability (Stream 4)	Step
IDV(8)	A, B, C Feed Composition (Stream 4)	Random Variation
IDV(9)	D Feed Temperature (Stream 2)	Random Variation
IDV(10)	C Feed Temperature (Stream 4)	Random Variation
IDV(11)	Reactor Cooling Water Inlet Temperature	Random Variation
IDV(12)	Condenser Cooling Water Inlet Temperature	Random Variation
IDV(13)	Reaction Kinetics	Slow Drift
IDV(14)	Reactor Cooling Water Valve	Sticking
IDV(15)	Condenser Cooling Water Valve	Sticking
IDV(16)	Unknown	
IDV(17)	Unknown	
IDV(18)	Unknown	
IDV(19)	Unknown	
IDV(20)	Unknown	
IDV(21)	The valve for Stream 4 was fixed at the steady state position	Constant Position

the data from the rest of the examples are treated as the testing set.

In Example 1, 200 observations for measured variable q are simulated under the normal distribution with mean zero and variance one. The variable has been normalized by its absolute minimum and maximum values (see Fig. 1a).

With the window size is specified as $b=20$, the historical distribution $p^q_{\mathrm{h},t}$ is calculated for $t=n-b+1$ to n, where $n=200$. The KLID between the historical distribution for q and a flat distribution (often called a uniform distribution, i.e., $\hat{p}(x)=1$)

$$f^q_{\mathrm{h},t} = I(p^q_{\mathrm{h},t}, 1), \tag{2}$$

is calculated based on numerical integration. If $p^q_{\mathrm{h},t}$ is a flat distribution, then $f^q_{\mathrm{h},t}$ is equal to zero. Fig. 1b shows that $f^q_{\mathrm{h},t}$ ranges from 1.3 to 2.1, indicating that the distribution is clearly different from a flat distribution.

For recent observations simulated under the same normal operating conditions as in Example 1, $f^q_{\mathrm{r},t}$ is expected to fall inside the same range as $f^q_{\mathrm{h},t}$. To verify that, another 200 observations for measured variable q are simulated in Example 2 under the same condition. The testing data for variable q has been normalized by the absolute minimum and maximum values used in Example 1 (see Fig. 2).

Using the same window size $b=20$, the recent distribution $p^q_{\mathrm{r},t}$ is calculated for $t=n-b+1$ to n in Example 2. The KLID between $p^q_{\mathrm{r},t}$ and a flat distribution is

$$f^q_{\mathrm{r},t} = I(p^q_{\mathrm{r},t}, 1), \tag{3}$$

and the result is shown in Fig. 2b. The range for $f^q_{\mathrm{r},t}$ is similar to the range for $f^q_{\mathrm{h},t}$, indicating that the distributions for q may be similar in both examples.

In Example 3, a fault condition is introduced at $t=30$, in which the variation of variable q decreases (see Fig. 3a). Fig. 3b shows that $f^q_{\mathrm{r},t}$ increases to 4.8 at $t=55$, indicating that the distribution has deviated from the normal conditions in Example 1. The small variations of q for $t>55$ is reflected in $f^q_{\mathrm{r},t}$, which also

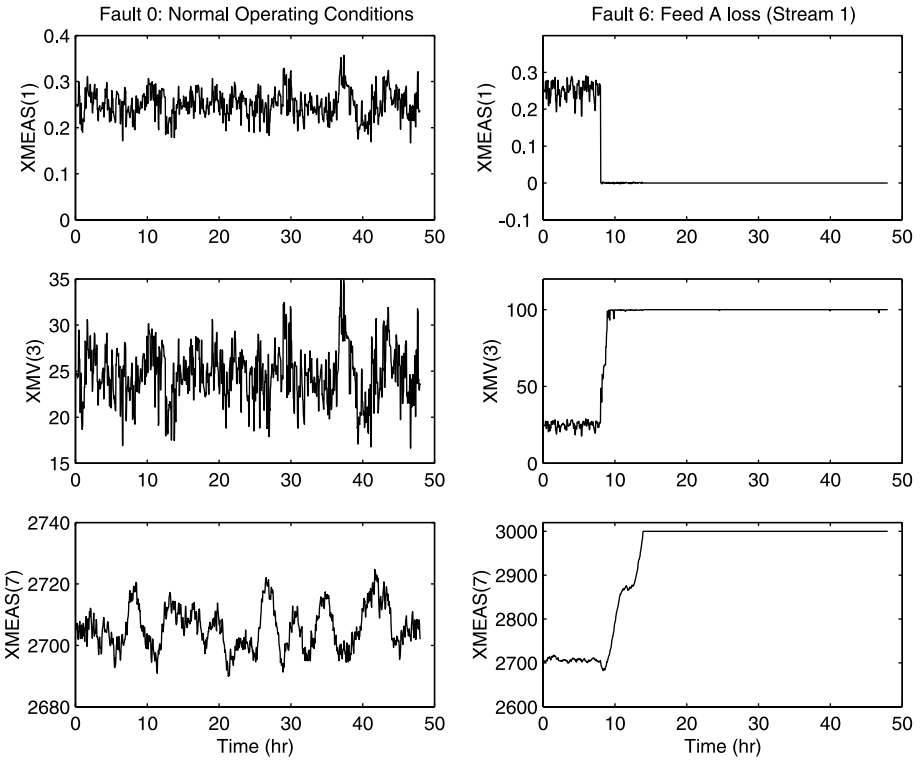

Fig. 6. Comparison of the A feed flow rate in Stream 1, XMEAS(1), the A feed valve in Stream 1, XMV(3), and the reactor pressure, XMEAS(7), for Faults 0 and 6. The fault occurs at $t=8$ h.

shows smaller variations for $t>55$. The detection delay is about 17 in this example. In general, a large window size b will result in a large detection delay, while a small window size b will result in a less sensitive fault detection statistic.

In Example 4, the variables drift for $t \geq 30$ (see Fig. 4a). The ranges for $f_{r,t}^q$ in both examples are very similar to the range of $f_{h,t}^q$, suggesting that $f_{r,t}^q$ is not sensitive in detecting shifts in mean. A statistic based solely on $f_{r,t}^q$ is not able to detect the changes effectively in Examples 3 and 4.

Examples 1 and 2 illustrate that similar KLIDs are obtained when the variable is associated with similar operating conditions. Examples 3 to 4 illustrate that $f_{r,t}^q$ is sensitive for detecting changes in the variance of a variable, but insensitive for detecting drift in a variable. KLID depends only on the distribution $p_{r,t}^q$ and the magnitude of the variable is not taken into account directly. This motivates the incorporation of additional measures for detecting faults.

In most cases, the effect of the faulty conditions on the variables is reflected in the mean of the variables or the range of the variables.

For recent observations in a window with size b, the mean of the variable q at current time $t=T$ is

$$m_{r,t}^q = \frac{1}{b}\sum_{t=T-b+1}^{T} q_t, \tag{4}$$

where q_t is the observation for q at time t. Alternatively, the shift in mean can be detected using cumulative sum chart (CUSUM) or an exponentially weighted moving average chart (EWMA) [24–26]. The range of the variable q is

$$s_{r,t}^q = \max_{T-b+1\leq t\leq T} q_t - \min_{T-b+1\leq t\leq T} q_t. \tag{5}$$

In Example 3, $s_{r,t}^q$ drops to nearly zero for $t>50$ (see Fig. 3d), indicating that $s_{r,t}^q$ will be able to detect the change in Example 3. In Example 4, $m_{r,t}^q$ indicates that the variable is drifting (see Fig. 4c). Incorporating $f_{r,t}^q$, $m_{r,t}^q$, and $s_{r,t}^q$ can provide a more sensitive fault detection statistic than the SELMON statistics in Section 2.1.

A normalization is used for $f_{r,t}^q$, $m_{r,t}^q$, and $s_{r,t}^q$ to compare between a recent distribution and a historical distribution. With f_h^q defined as the $I(f_{h,t}^q,1)$ with the window size b, the adjusted $f_{r,t}^q$ is defined by

$$\tilde{f}_{r,t}^q = |f_{r,t}^q - f_h^q|, \tag{6}$$

with this step, the positive and negative shifts from the historical distribution can be detected. The normalized KLID is defined by

$$F_{r,t}^q = \frac{\tilde{f}_{r,t}^q}{\mathrm{mean}(\tilde{f}_{h,t}^q) + n_r \mathrm{std}(\tilde{f}_{h,t}^q)}, \tag{7}$$

where std denotes standard deviation, $\tilde{f}_{h,t}^q = |f_{h,t}^q - f_h^q|$, and n_r is a constant used to specify the type-I error, which can be determined based on the historical data. For a large-scale system, a higher n_r is desired in order to achieve a lower overall false alarm rate. Alternatively, $\tilde{f}_{r,t}^q$ can be divided by the maximum value of $\tilde{f}_{h,t}^q$ to obtain the normalization.

Similarly, the adjusted $m_{r,t}^q$ is defined by

$$\tilde{m}_{r,t}^q = |m_{r,t}^q - m_h^q|, \tag{8}$$

where m_h^q is the mean of variable q in the entire training set, which is equal to 0.5. The adjusted $s_{r,t}^q$ is defined by

$$\tilde{s}_{r,t}^q = |s_{r,t}^q - s_h^q|, \tag{9}$$

where s_h^q is the range of the variable q in the entire training set.

Table 2
The false alarm rate (type-I error) for the testing set of Fault 0 and the missed detection rates (type-II error) for the testing sets for Faults 1–21 using the modified distance (models derived based on training set for Fault 0, which contains 480 observations)

Fault	DI	CD	DI/CD
0	0.026	0.0200	0.0462
1	0.009	0.0012	0.003
2	0.020	0.013	0.013
3	0.890	0.928	0.866
4	0	0	0
5	0.006	0	0
6	0.005	0	0
7	0	0	0
8	0.031	0.011	0.015
9	0.903	0.934	0.885
10	0.174	0.153	0.080
11	0.008	0.175	0.006
12	0.004	0.003	0.003
13	0.051	0.051	0.050
14	0.001	0	0
15	0.774	0.824	0.751
16	0.254	0.088	0.051
17	0.029	0.043	0.026
18	0.108	0.094	0.095
19	0.068	0.441	0.036
20	0.106	0.130	0.080
21	0.056	0.476	0.056
Overall	0.166	0.208	0.144

The normalized $m^q_{r,t}$and $s^q_{r,t}$are defined by

$$M^q_{r,t} = \frac{\tilde{m}^q_{r,t}}{\text{mean}(\tilde{m}^q_{h,t}) + n_r \text{std}(\tilde{m}^q_{h,t})}, \quad (10)$$

and

$$S^q_{r,t} = \frac{\tilde{s}^q_{r,t}}{\text{mean}(\tilde{s}^q_{h,t}) + n_r \text{std}(\tilde{s}^q_{h,t})}, \quad (11)$$

respectively.

The modified DI is defined by

$$DI^q_t = \left\| \begin{bmatrix} F^q_{r,t} \\ C^q_{r,t} \\ F^q_{r,t} C^q_{r,t} \end{bmatrix} \right\|, \quad (12)$$

where $C^q_{r,t}$ takes the larger value between $M^q_{r,t}$ and $S^q_{r,t}$. Note that either $S^q_{r,t}$ or $M^q_{r,t}$ contributes to the modified DI. For most observable faults (see Figs. 3c,d and 4c,d), faulty conditions do not usually effect both $s^q_{r,t}$ and $m^q_{r,t}$, so including both terms in the modified DI would result in a less sensitive fault detection statistic.

To use DI^q_t for fault detection, a pre-specified threshold based on the training data associated with the normal operating conditions is required. The thresholds for $F^q_{r,t}$, $M^q_{r,t}$, and $S^q_{r,t}$ are one. Therefore, the threshold for DI^q_t is specified as $\sqrt{3}$.

Recall that Example 2 is associated with the testing set for the normal operating conditions. It is expected that the distance measure DI^q_t should be less than the threshold for nearly all observations. Calculations show that the false alarm rate for DI^q_t is small (1/180), indicating that the threshold is well-defined. The normalized modified distance is able to detect the faults promptly for Examples 3 and 4.

The modified distance measure is used to detect a change in the frequency distribution for each measure variable. To quantify the similarity between each causal relationship associated with the causal map under current operating conditions and historical normal operating conditions, the causal dependence (CD) is used.

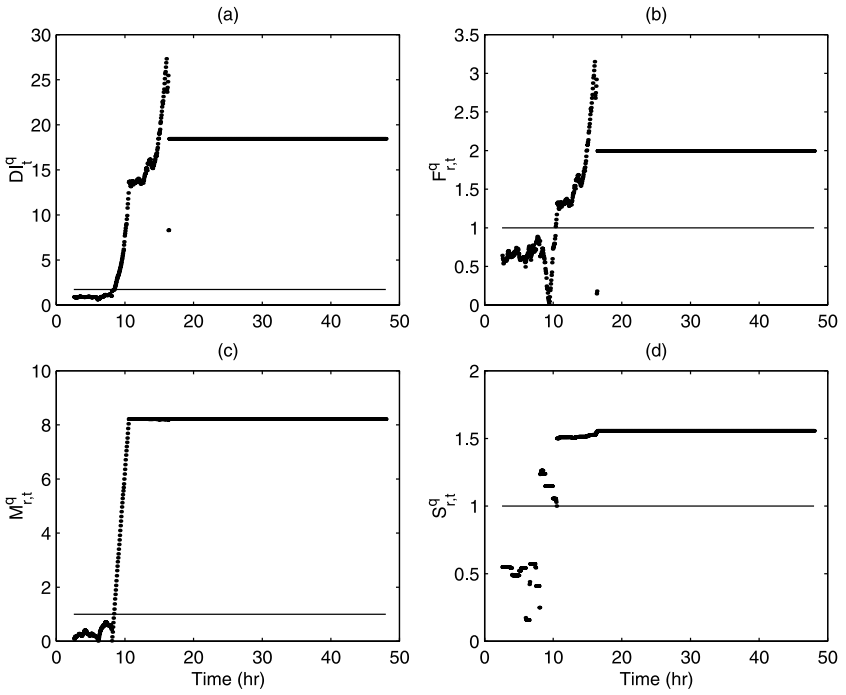

Fig. 7. (a) The modified distance, (b) the normalized KLID, (c) the normalized mean, and (d) the normalized range of the *A* feed flow rate in Stream 1, XMEAS(1), for Fault 6. The fault occurs at $t = 8$ h. The solid line represents the threshold.

For causal dependency, define c as the cause variable and e as the effect variable. The CD is based on the multivariate T^2 statistic, which is defined by

$$\mathrm{CD}_{c,e} = T^2_{c,e} = (\mathbf{y} - \bar{\mathbf{y}})^T S^{-1}_{c,e} (\mathbf{y} - \bar{\mathbf{y}}), \tag{13}$$

where $\mathbf{y}=[c\ e]^T$, $\bar{\mathbf{y}}$ is the mean of $\mathbf{y}$, and $S_{c,e}$ is the sample covariance for variables c and e. Full rank is taken for the T^2 statistic. The threshold for $T^2_{c,e}$ is

$$\mathrm{CD}_\alpha = T^2_\alpha = \frac{2(n-1)(n+1)}{n(n-2)} F_\alpha(2, n-2), \tag{14}$$

where n is the number of observations in the training sets and α is the level of significance [27]. Assuming that c and e follow a normal distribution, a false alarm rate α is expected for the T^2 statistic. Let the total number of causal dependencies in the process be n_{CD}, then the overall type-I error is

$$\alpha_{\mathrm{total}} = 1 - (1-\alpha)^{n_{\mathrm{CD}}}. \tag{15}$$

For small n_{CD}, α_{total} is comparable with α; for large n_{CD}, α_{total} is larger than α. For fault detection, the desired type-I error α_{total} is first specified, then the threshold T^2_α for each causal dependency is calculated using Eqs. (14) and (15).

The training data associated with the normal operating conditions (denoted as Fault 0) is required for fault detection. The data in the training set, consisting of m observation variables and n observations for each variable, are stacked into a matrix $X \in \Re^{n \times m}$, given by

$$X = \begin{bmatrix} x_{11} & x_{12} & \dots & x_{1m} \\ x_{21} & x_{22} & \dots & x_{2m} \\ \vdots & \vdots & \dots & \vdots \\ x_{n1} & x_{n2} & \dots & x_{nm} \end{bmatrix}. \tag{16}$$

With the window size specified for each variable, the historical distribution $p^q_{\mathrm{h},t,0}$, the mean $m^q_{\mathrm{h},t,0}$, and the range $s^q_{\mathrm{h},t,0}$ associated with each variable are com-

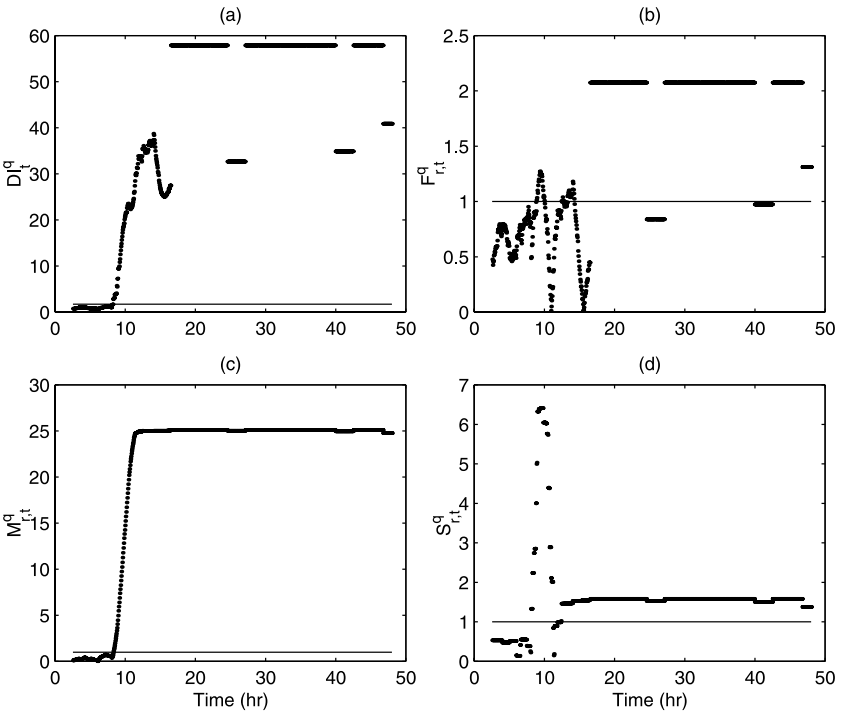

Fig. 8. (a) The modified distance, (b) the normalized KLID, (c) the normalized mean, and (d) the normalized range of the A feed valve in Stream 1, XMV(3), for Fault 6. The fault occurs at $t=8$ h. The solid line represents the threshold.

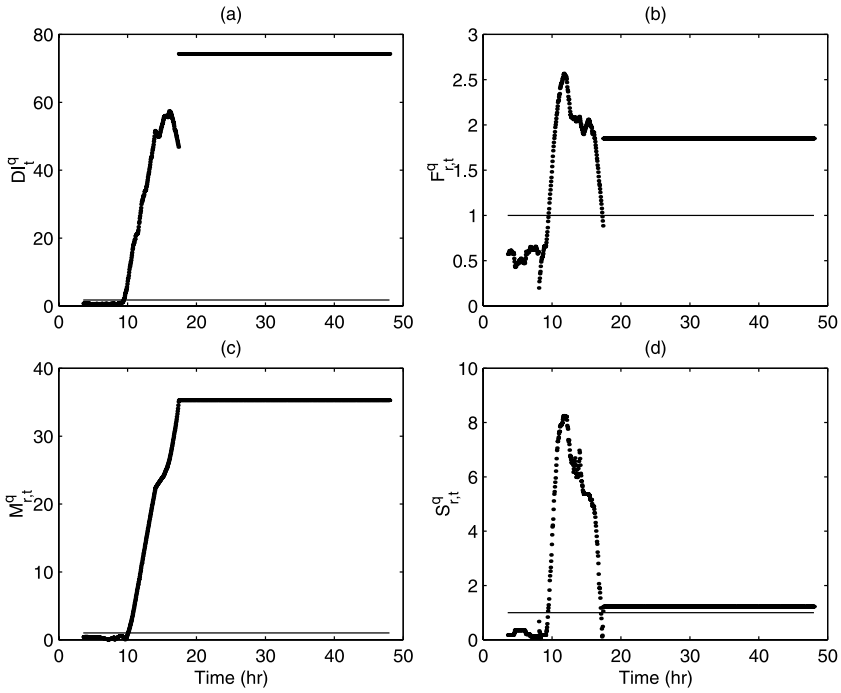

Fig. 9. (a) The modified distance, (b) the normalized KLID, (c) the normalized mean, and (d) the normalized range of the reactor pressure, XMEAS(7), for Fault 6. The fault occurs at $t=8$ h. The solid line represents the threshold.

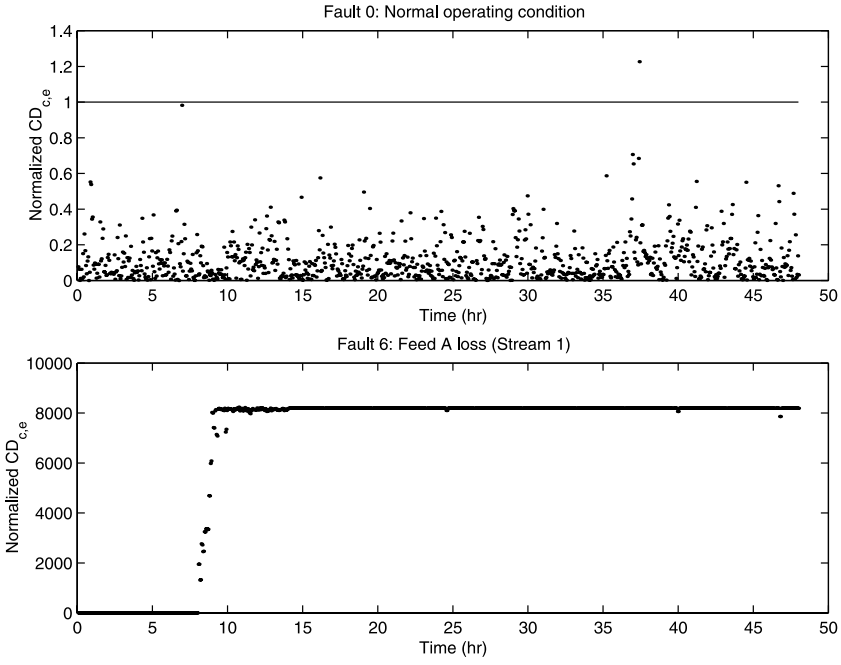

Fig. 10. The normalized CD based on the *A* feed flow rate in Stream 1 and the *A* feed valve in Stream 1 for Faults 0 and 6. The fault occurs at $t=8$ h. The solid line represents the threshold.

puted. In addition, $p^q_{h,0}$, $m^q_{h,0}$, and $s^q_{h,0}$ are computed using n observations for each variable. A fault associated with a sensor or sensor changing its character is detected for the variable q if

$$DI^q_t > DI_\alpha. \tag{17}$$

To detect broken causal dependencies among variables, a causal map containing the causal relationship between all of the measured variables is required. The causal map can be derived based on knowledge from a plant engineer. The sample covariance matrix from the normal data can be used to verify the accuracy of the causal map. Two variables are related when the correlation is high. Based on the training data for Fault 0, the sample covariance $S_{c,e}$ and the mean of the variable $\bar{\mathbf{y}}=[c\ e]^T$ are computed for each causal dependency. The threshold is calculated using Eqs. (14) and (15). The causal relationship between two variables is broken when

$$T^2_{c,e} > T^2_\alpha, \tag{18}$$

and Eq. (17) is satisfied for variables c and e. In other words, the causal relationship remains normal for c and e as long as Eq. (17) is satisfied for either variables.

When a fault is detected, the variables c and e which satisfy Eqs. (17) and (18) represent the fault propagation path (denoted as FP_t). Such fault propagation information plays an important role in isolating and determining the root cause.

Once a fault has been detected, the next step is to determine the cause of the out-of-control status. The task of diagnosing the fault can be rather challenging when the number of process variables is large, and the

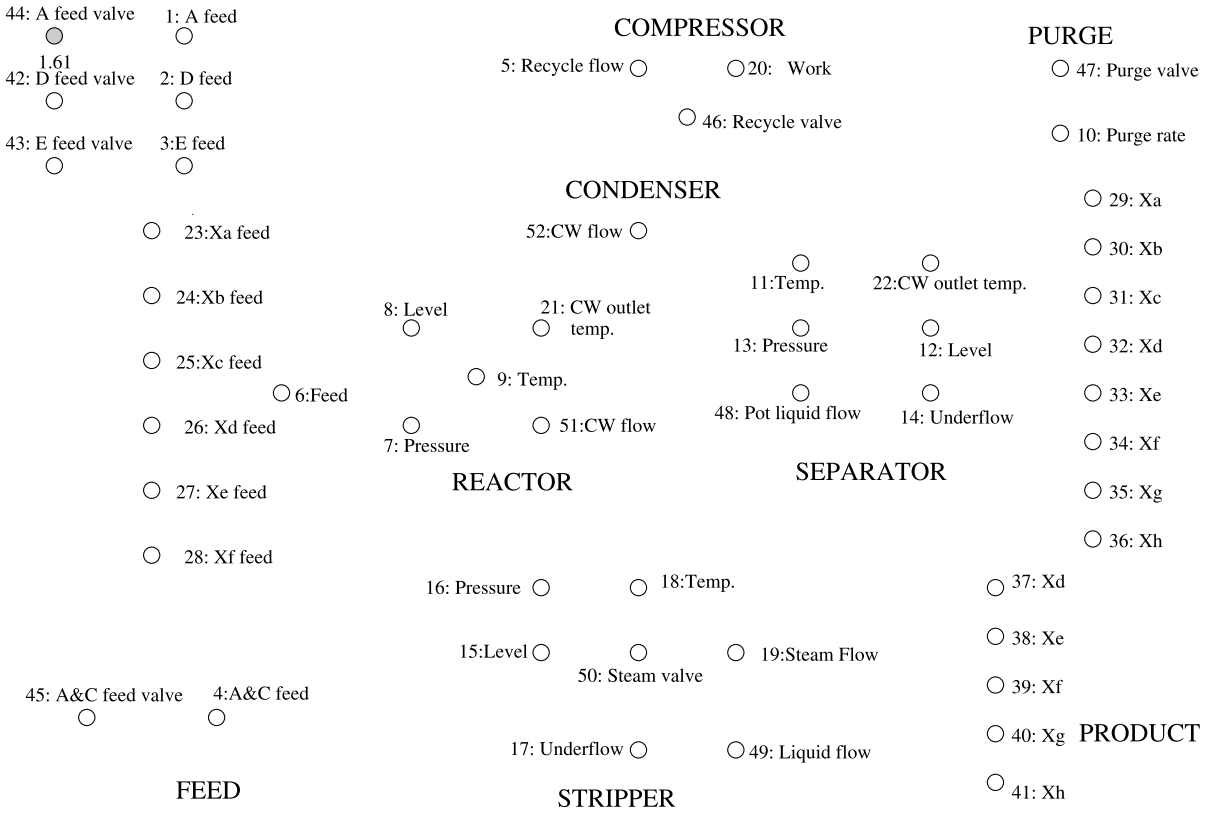

Fig. 11. Fault propagation path at $t=8.25$ h (15 min after Fault 6 occurs). Grey node represents the variable that has highest DI.

process is highly integrated. Also, many of the measured variables may deviate from their set-points for only a short time period when a fault occurs, due to control loops bringing the variables back to their set-points (even though the fault is persisting in the system). This type of systems behavior can disguise the fault, making it difficult for an automated fault diagnosis algorithm to correctly isolate the correct fault acting on the system.

The goal of fault identification is to identify the variables which are most related with the fault origin, thereby focusing the plant operators and engineers on the subsystem(s) most likely where the fault occurred. This assistance provided by the fault identification scheme in locating the fault can effectively incorporate the operators and engineers in the process monitoring scheme and significantly reduce the time to recover in-control operations. The magnitudes of the DI and CD represent the degree to which the variables have deviated from their distributions in the normal operating conditions. Root causes are often highly correlated with the variables which have the highest DI and the causal dependency which has the highest CD. Proper and immediate actions to those variables can prevent the effect of the fault from propagating to other variables.

3. Application

3.1. Tennessee Eastman process

The process simulator for the Tennessee Eastman process (TEP) was created by the Eastman Chemical to provide a realistic industrial process for evaluating

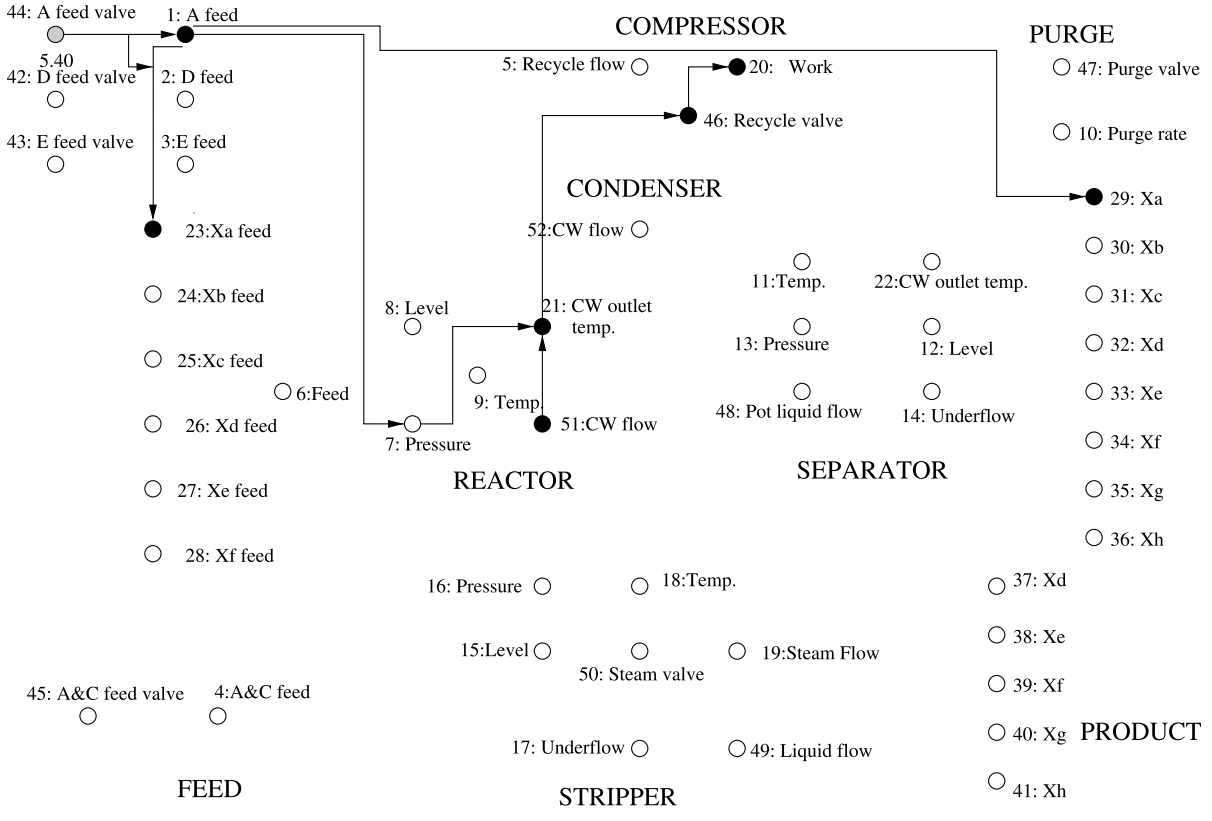

Fig. 12. Fault propagation path at $t = 9$ h (1 h after Fault 6 occurs). Grey node represents the variable that has the highest DI, black node represents broken variable, and arc represents broken causal dependencies.

process control and monitoring methods [28]. The TE process simulator has been widely used by the process monitoring community as a source of data for comparing various approaches [1–3,7,8,29–40].

The chemical plant simulator is based on an industrial process where the components, kinetics, and operating conditions were modified for proprietary reasons (see Fig. 5). The gaseous reactants A, C, D, and E and the inert B are fed to the reactor where the liquid products G and H are formed. The reactions in the reactor are irreversible, exothermic, and approximately first-order with respect to the reactant concentrations. The reactor product stream is cooled through a condenser and then fed to a vapor–liquid separator. The vapor exiting the separator is recycled to the reactor feed through the compressor. A portion of the recycle stream is purged to keep the inert and byproducts from accumulating in the process. The condensed components from the separator (Stream 10) are pumped to the stripper. Stream 4 is used to strip the remaining reactants in Stream 10, and is combined with the recycle stream. The products G and H exiting the base of the stripper are sent to a downstream process which is not included in this process. The simulation code allows 21 preprogrammed major process faults, as shown in Table 1. The plant-wide control structure recommended in Lyman and Georgakis [41] was implemented to generate the closed loop simulated process data for each fault.

One simulation run (Fault 0) was generated with no faults for the training set. No training sets were generated for Faults 1–21. The simulation time for each run was 25 h.

The data in the testing set consisted of 22 different simulation runs, where the random seed was changed between each run. The first 16 simulation runs directly

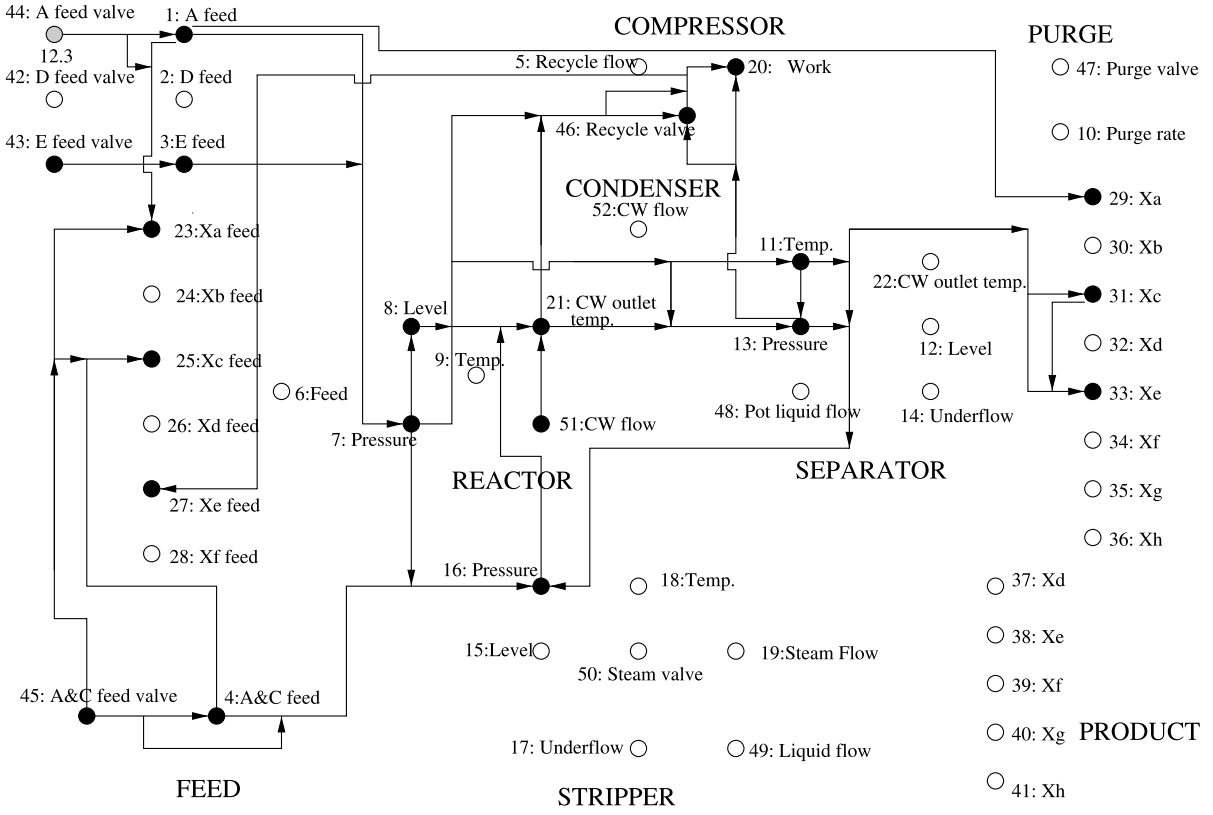

Fig. 13. Fault propagation path at $t=10$ h (2 h after Fault 6 occurs). Grey node represents the variable that has the highest DI, black node represents broken variable, and arc represents broken causal dependencies.

correspond to the runs in the training set (Faults 0–15). One simulation run (Fault 21) was generated by fixing the position of the valve for Stream 4 at the steady state position. Five more simulation runs (Faults 16–20) were simulated under unknown conditions, specified by the original TEP simulator. The simulation time for each run was 48 h. The simulation started with no faults, and the faults were introduced 8 simulation h into the run. The total number of observations generated for each run was $n = 960$.

The causal map can be constructed in a straightforward manner using a fundamental mathematical model of the process. Because a fundamental model of the TEP is assumed to be unavailable, the causal model used in this work was constructed based on the knowledge of the process and the correlation coefficients associated with the data from normal operating conditions.

3.2. Case studies

Selective case studies are discussed here to illustrate the proficiency of the proposed algorithm. Detailed discussion of the results are available [22].

3.2.1. Fault 6

For Fault 6, there is a feed loss of *A* in Stream 1 at $t = 8$ h (see XMEAS(1) in Fig. 6), which causes the control loop on Stream 1 to fully open the *A* feed valve (see XMV(3) in Fig. 6). Because there is no reactant *A* in the feed, the reaction will eventually stop. This causes the gaseous reactants D and E build up in the reactor, and hence the reactor pressure increases (see XMEAS(7) in Fig. 6). The reactor pressure continues to increase until it reaches the safety limit of 2950 kPa, at this point the valve for Control Loop 6 is fully open. Clearly, it is very

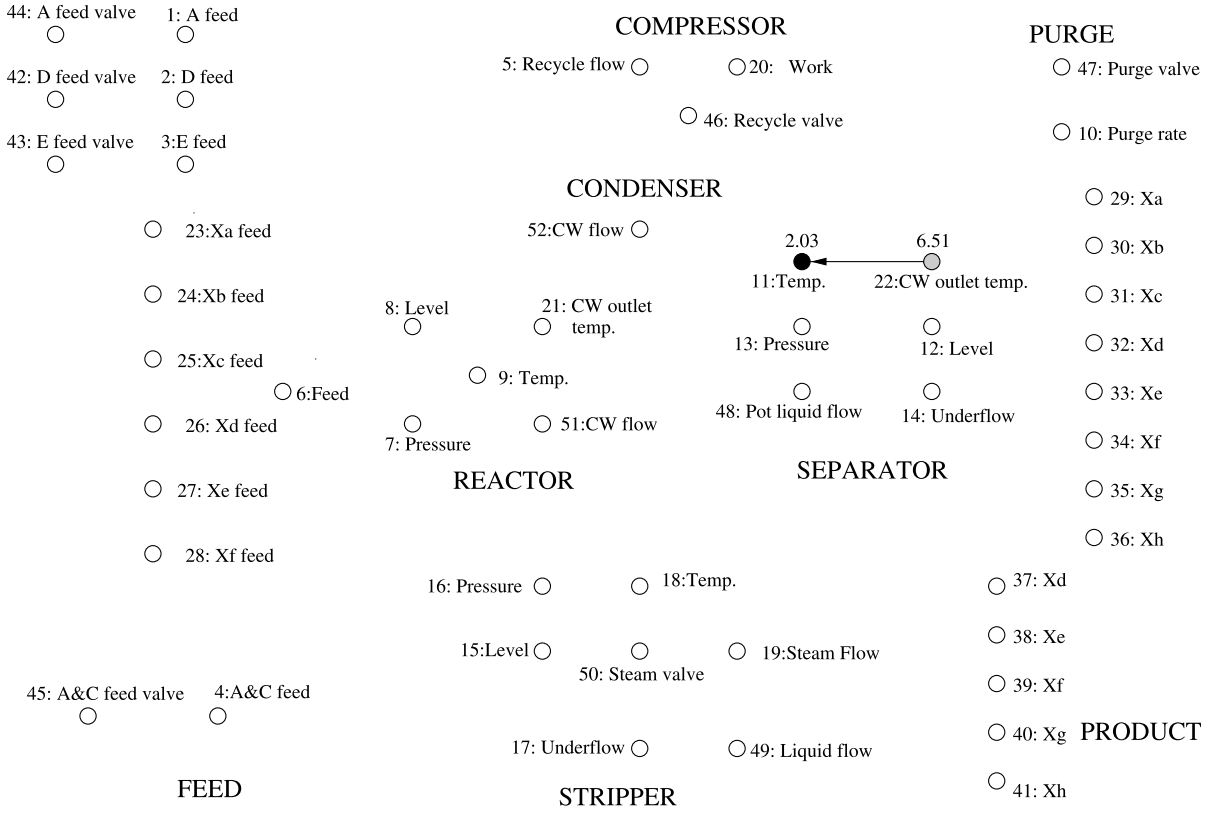

Fig. 14. Fault propagation path at $t = 13$ h (5 h after unknown Fault 18 occurs). Grey node represents the variable that has the highest DI, black node represents broken variable, and arc represents broken causal dependencies.

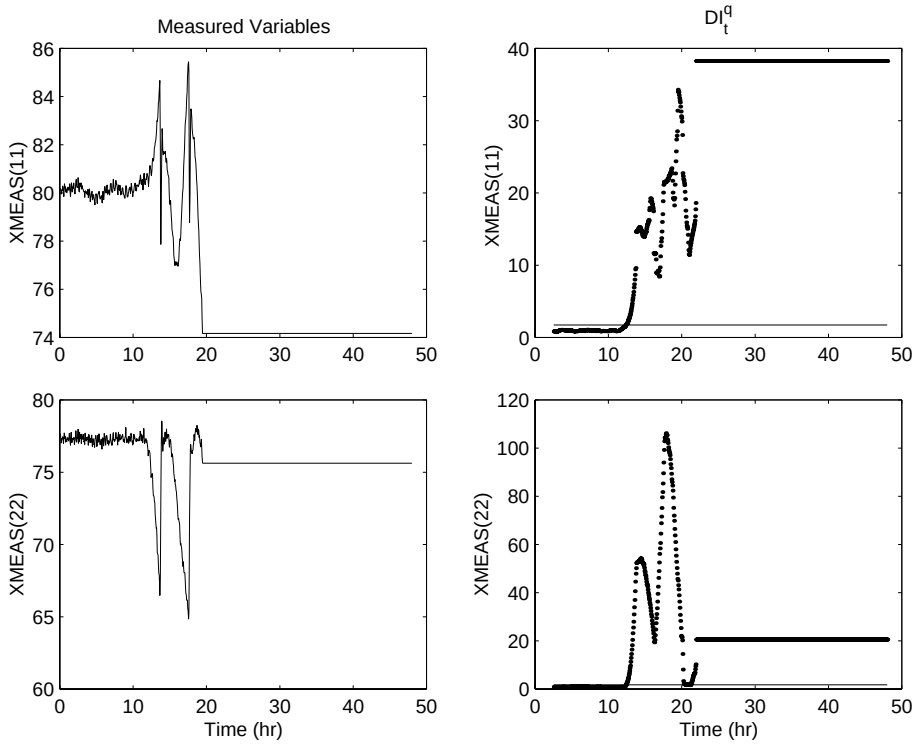

Fig. 15. Measured variables and the modified distances of the product separator temperature, XMEAS(11), and the separator cooling water outlet temperature, XMEAS(22), for Fault 18. The fault occurs at $t=8$ h. The solid line represents the threshold.

important to detect this fault promptly before the fault upsets the whole process.

The DI and CD detect Fault 6 effectively (see Table 2). Fig. 7 shows that the modified distance increases up to 28 for the *A* feed flow rate, which is 16 times the threshold. The *A* feed flow rate decreases from about 0.25 to 0 at $t=8$ h (see Fig. 6) and it remains steady at 0 for $t>8$ h. Because the mean and range of the *A* feed flow rate change significantly, the normalized mean and the normalized range both promptly detect the fault. The flat distribution for $t>8$ h is also detected by the KLID.

Similarly to the *A* feed flow rate in Stream 1, extreme changes associated with the mean, range, and distribution are found in the *A* feed valve in Stream 1 and the reactor pressure (see Figs. 8 and 9). As a result, the KLID, the normalized mean, and the normalized range are able to detect Fault 6 promptly (see Fig. 7).

The $CD_{c,e,}$ associated with the *A* feed valve and the *A* feed flow rate is shown in Fig. 10. The CD increases up to 8000 times the threshold, indicating extreme changes in the means for these two variables.

Fig. 11 shows the fault propagation path 15 min (five sampling intervals) after the fault occurs, the normalized modified distance for the *A* feed valve in Stream 1 is 1.61. The normalized modified distance is less than one for the rest of the variables. The feed

Table 3
The number of broken nodes in the fault propagation path for Fault 18

Time (h)	Number of broken nodes
12	0
13	2
13.25	9
13.5	13
13.75	23
14	27
15	34
20	42
32	51
48	51

valve for *A* is promptly identified as the root cause for Fault 6.

Fig. 12 shows the fault propagation path 1 h after the fault occurs. The effects of Fault 6 propagate to other variables. The normalized modified distance for the *A* feed valve has the highest magnitude, which is 5.40. Two hours after Fault 6 occurs, the normalized modified distance for 21 out of 52 variables are larger than one (see Fig. 13), indicating that the fault has deeply affected most variables. The normalized modified distance for the *A* feed valve further increases to 12.3, which continues to represent the highest score among all 52 variables. The number of broken variables in the fault propagation path increases to 38 and 46, respectively, after 5 and 20 h have passed. This example is effective in illustrating the importance in promptly detecting and identifying the fault using the modified distance before the whole process is being upset. This also shows that the modified distance can promptly and effectively identify the fault, and that a visualization of the fault propagation path constructed from these statistics can be valuable for operators to understand how the fault is affecting the process.

3.2.2. Fault 18

The author of the Tennessee Eastman plant simulator purposely does not reveal the root causes for the unknown Faults 16 to 20. The fault propagation paths can provide useful information to reveal the root causes in these cases. For 5 h after Fault 18 occurs ($t = 8$ to 13 h), all 52 variables behave normally and no broken nodes are recorded in the fault propagation path. At $t = 13$ h, the nodes for the separator temperature, XMEAS(11), and the separator cooling water outlet temperature, XMEAS(22), are broken (see Fig. 14). The arcs between the variables are also broken. Fig. 15 confirms that the separator behaves abnormally. The effect of Fault 18 is severe and the control loops are not

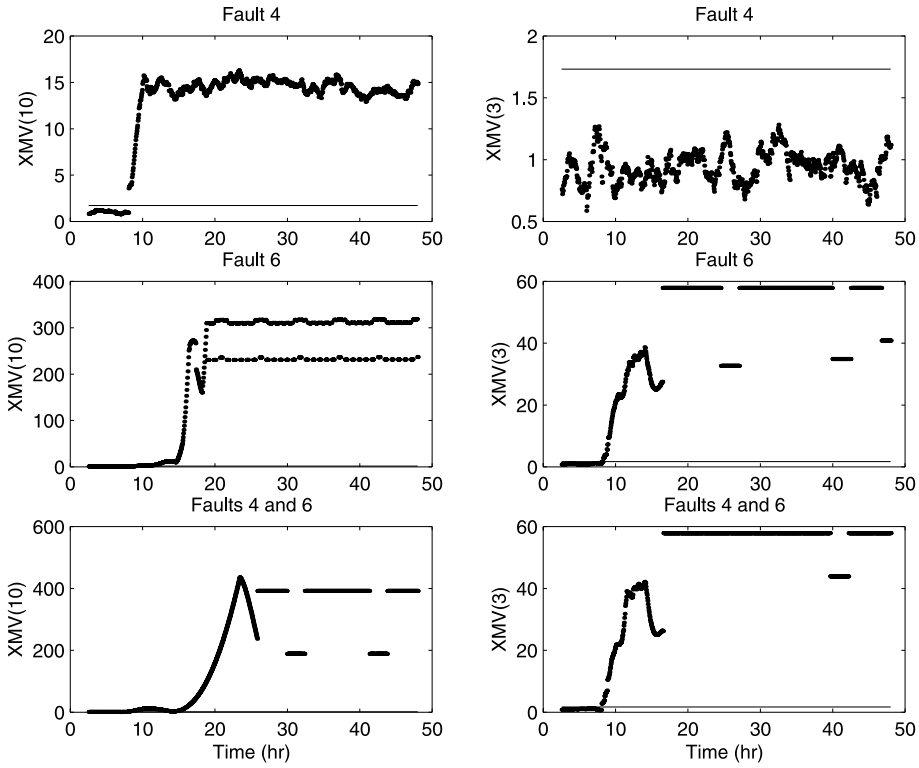

Fig. 16. The modified distance of the reactor cooling water flow rate, XMV(10), and the *A* feed valve in Stream 1, XMV(3), for Fault 4, Fault 6, and multiple Faults 4 and 6. The faults occur at $t = 8$ h. The solid line represents the threshold.

able to compensate for the fault. At $t = 14$ h, 27 broken nodes are recorded in the fault propagation path (see Table 3); at $t = 32$ h, 51 out of 52 nodes are broken. The modified distance is able to identify and isolate Fault 18 before the whole process is upset.

3.2.3. Multiple Faults 4 and 6

Multiple Faults 4 and 6 are masked multiple faults, in which the variables affected by one fault are a subset of the variables affected by another fault. The previous discussions show that Fault 6 involves unsteady operations, causing most variables to deviate significantly from their normal behaviors. Although Fault 4 has a clear effect on the reactor cooling water flow rate, the effect of Fault 4 is masked when multiple Faults 4 and 6 occur. This is confirmed by the modified distances for the reactor cooling water flow rate and the *A* feed valve in Stream 1 (see Fig. 16).

Three minutes after multiple Faults 4 and 6 occur two disjointed fault propagation paths appear (see Fig. 17). This is an indication that multiple faults occurred. The fault propagation path containing the reactor temperature and the reactor cooling water outlet temperature represents the symptoms for Fault 4, while the fault propagation path containing the *A* feed valve represents the symptom for Fault 6.

Forty five minutes after the faults occur, the number of variables in one fault propagation increases to three, while the number of variables in the other fault propagation remain the same (see Fig. 18). This shows that Fault 6 has propagated to more variables. Seventy five minutes after the faults occur, the total number of variables in the fault propagation path increases to 9, in which Fault 4 is masked by Fault 6.

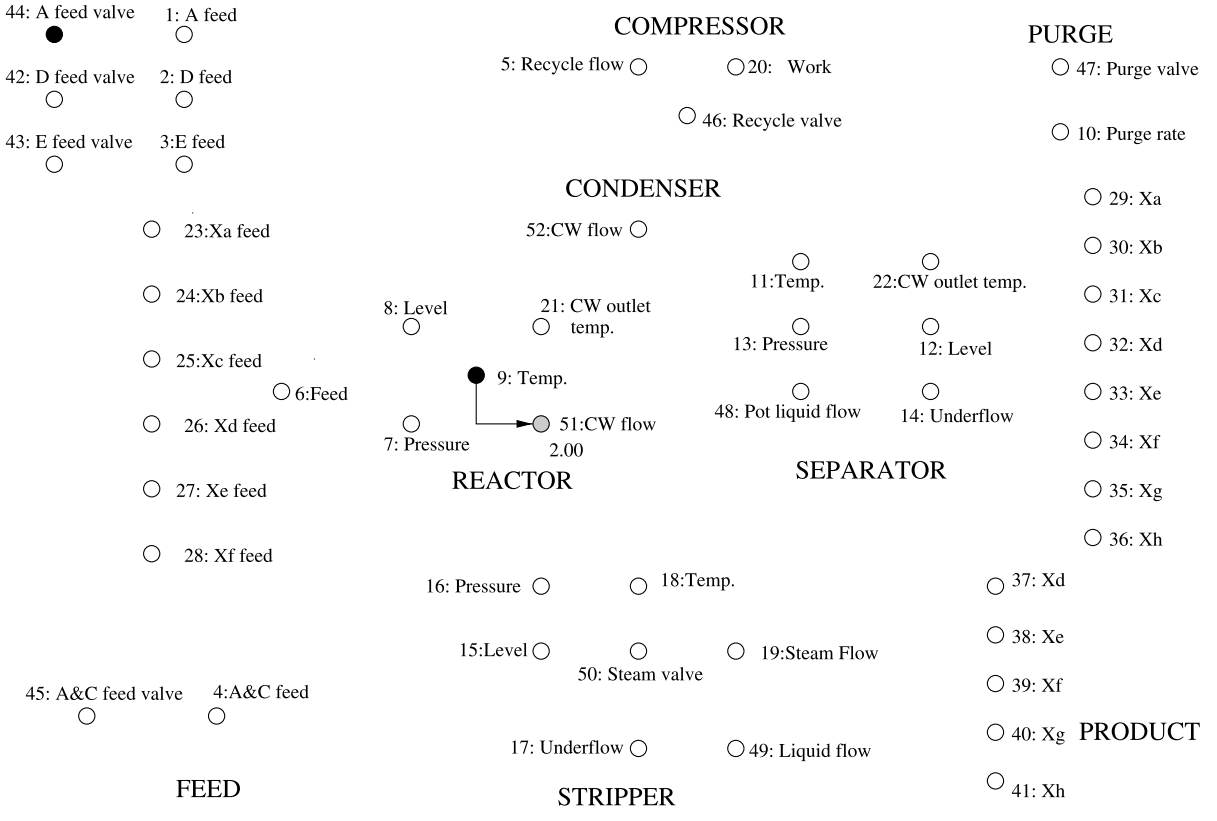

Fig. 17. Fault propagation path at $t = 8.05$ h (3 min after multiple Faults 4 and 6 occur). Grey node represents the variable that has the highest DI, black node represents broken variable, and arc represents broken causal dependencies.

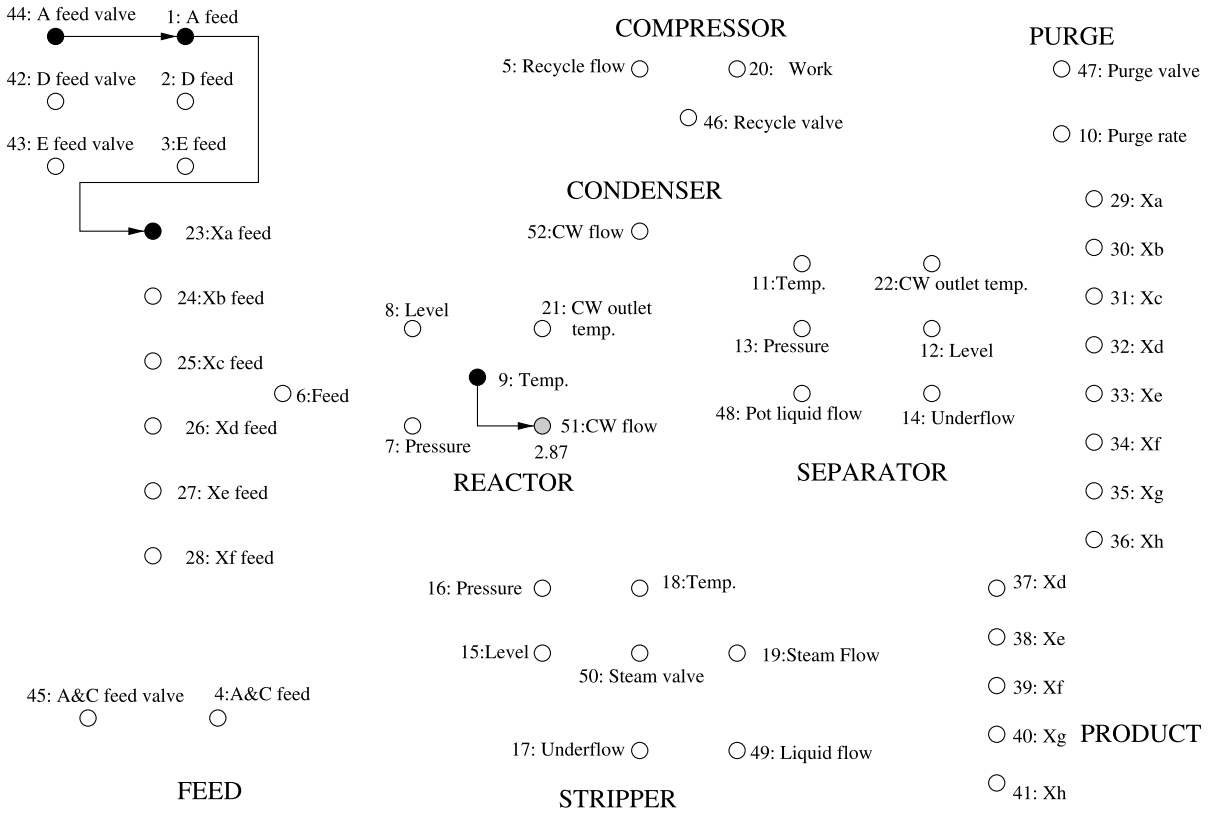

Fig. 18. Fault propagation path at $t = 8.25$ h (15 min after multiple Faults 4 and 6 occur). Grey node represents the variable that has the highest DI, black node represents broken variable, and arc represents broken causal dependencies.

3.3. Overall fault detection performance

The missed detection rates for DI and CD are comparable for all fault classes (see Table 2), except Faults 11 and 21 in which DI outperforms CD. The overall missed detection rate using DI/CD is 0.144. When the unobservable Faults 3, 9, and 15 are not considered in the overall missed detection rate, the number drops to 0.029. With this exceptionally low overall missed detection rate compared to other methods [22], the DI/CD is recommended for use in fault detection.

4. Conclusions

The modified distance (DI) and modified causal dependency (CD) were proposed to incorporate with the data-driven approach and the causal map to improve the proficiency for identifying and diagnosing faults. The DI is based on the Kullback–Leibner information distance (KLID), the mean of the measured variables, and the range of the measured variables. The CD is derived based on the multivariate T^2 statistic. The DI/CD algorithm outperformed the purely data-driven techniques such as PCA for detecting and identifying known, unknown, and multiple faults using the data sets from the Tennessee Eastman process [22]. The DI/CD algorithm is especially well-suited for identifying faults. The fault propagation path identified the root causes for all known faulty cases in the Tennessee Eastman process. This valuable information allows the plant operators to focus on the subsystems in which the fault has originated and allows them to react quickly before the fault upsets the whole process. The fault propagation path also reveals the dynamics and the effects of the fault on the variables. Such information is especially important in fault prevention and quality improvement.

Acknowledgements

This work was supported by International Paper and the National Center for Supercomputing Applications. The authors would like to thank Randy Pell at the Dow Chemical Company for his comments, which significantly improved the paper.

References

[1] L.H. Chiang, E.L. Russell, R.D. Braatz, Fault Detection and Diagnosis in Industrial Systems, Springer Verlag, London, 2001.
[2] E.L. Russell, L.H. Chiang, R.D. Braatz, Data-driven Techniques for Fault Detection and Diagnosis in Chemical Processes, Springer Verlag, London, 2000.
[3] E.L. Russell, L.H. Chiang, R.D. Braatz, Fault detection in industrial processes using canonical variate analysis and dynamic principal component analysis, Chemometrics and Intelligent Laboratory Systems 51 (2000) 81–93.
[4] R. Dunia, S.J. Qin, Joint diagnosis of process and sensor faults using principal component analysis, Control Engineering Practice 6 (1998) 457–469.
[5] T. Kourti, J.F. MacGregor, Multivariate SPC methods for process and product monitoring, Journal of Quality Technology 28 (1996) 409–428.
[6] B.R. Bakshi, Multiscale PCA with application to multivariate statistical process monitoring, AIChE Journal 44 (1998) 1596–1610.
[7] A.C. Raich, A. Cinar, Statistical process monitoring and disturbance diagnosis in multivariable continuous processes, AIChE Journal 42 (1996) 995–1009.
[8] W. Ku, R.H. Storer, C. Georgakis, Disturbance detection and isolation by dynamic principal component analysis, Chemometrics and Intelligent Laboratory Systems 30 (1995) 179–196.
[9] M. Iri, K. Aoki, E. O'Shima, H. Matsuyama, An algorithm for diagnosis of system failures in the chemical process, Computers & Chemical Engineering 3 (1979) 489–493.
[10] J. Shiozaki, H. Matsuyama, E. O'Shima, M. Iri, An improved algorithm for diagnosis of system failures in the chemical process, Computers & Chemical Engineering 9 (1985) 285–293.
[11] Y. Tsuge, J. Shiozaki, H. Matsuyama, E. O'Shima, Fault diagnosis algorithms based on the signed directed graph and its modifications, Industrial and Chemical Engineering Symposium Series 92 (1985) 133–144.
[12] I.P. Gal, K.M. Hangos, SDG model-based structures for fault detection, Proc. of the IFAC On-line Fault Detection and Supervision in the Chemical Process Industries, Piscataway, NJ, IEEE Press, 1998, pp. 243–248.
[13] D.J. Allen, Digraphs and fault trees, Industrial & Engineering Chemistry Fundamentals 23 (1984) 175–180.
[14] S.A. Lapp, G.J. Power, Computer-aided synthesis of fault tree, IEEE Transactions on Reliability 28 (1977) 2–13.
[15] W.G. Schneeweiss, Fault tree analysis in case of multiple faults, especially covered and uncovered ones, Microelectronics and Reliability 38 (1998) 659–663.
[16] T.F. Petti, J. Klein, P.S. Dhurjati, Diagnostic model processor. Using deep knowledge for process fault diagnosis, AIChE Journal 36 (1990) 565–575.
[17] J. Zhao, B. Chen, J. Shen, A hybrid ANN-ES system for dynamic fault diagnosis of hydrocracking process, Computers & Chemical Engineering 21 (1997) S929–S933.
[18] R.J. Doyle, Determining the loci of anomalies using minimal causal models, International Joint Conference on Artificial Intelligence, American Association for Artificial Intelligence, Montreal, Canada, 1995 (August), pp. 1a–7a.
[19] R.J. Doyle, L. Charest, N. Rouquette, J. Wyatt, C. Robertson, Causal modeling and event-driven simulation for monitoring of continuous systems, Computers in Aerospace 9 (1993) 395–405.
[20] R.J. Doyle, S.A. Chien, U.M. Fayyad, E.J. Wyatt, Focused real-time systems monitoring based on multiple anomaly models, 7th Int. Workshop on Qualitative Reasoning, Eastsound, Washington, May, 1993.
[21] E.L. Russell. Process Monitoring of Large Scale Systems. PhD thesis, University of Illinois, Urbana, IL, 1998.
[22] L.H. Chiang. Fault Detection and Diagnosis for Large-Scale Systems. PhD thesis, University of Illinois, Urbana, IL, 2001.
[23] L. Ljung, System Identification: Theory for the User, Prentice-Hall, Englewood Cliffs, NJ, 1987.
[24] P. Fasolo, D.E. Seborg, SQC approach to monitoring and fault detection in HVAC control systems, Proc. of the American Control Conf., Piscataway, NJ, vol. 3, IEEE Press, 1994, pp. 3055–3059.
[25] D.C. Montgomery, Introduction to Statistical Quality Control, Wiley, New York, 1985.
[26] B.A. Ogunnaike, W.H. Ray, Process Dynamics, Modeling, and Control, Oxford Univ. Press, New York, 1994.
[27] J.F. MacGregor, T. Kourti, Statistical process control of multivariate processes, Control Engineering Practice 3 (1995) 403–414.
[28] J.J. Downs, E.F. Vogel, A plant-wide industrial-process control problem, Computers & Chemical Engineering 17 (1993) 245–255.
[29] L.H. Chiang, E.L. Russell, R.D. Braatz, Fault diagnosis in chemical processes using Fisher discriminant analysis, discriminant partial least squares, and principal component analysis, Chemometrics and Intelligent Laboratory Systems 50 (2000) 243–252.
[30] A.C. Raich, A. Cinar, Multivariate statistical methods for monitoring continuous processes: assessment of discriminatory power disturbance models and diagnosis of multiple disturbances, Chemometrics and Intelligent Laboratory Systems 30 (1995) 37–48.
[31] A.C. Raich, A. Cinar, Process disturbance diagnosis by statistical distance and angle measures, Proc. of the 13th IFAC World Congress, Piscataway, NJ, IEEE Press, 1996, pp. 283–288.
[32] H.B. Aradhye, B.R. Bakshi, R. Strauss, Process monitoring by PCA, dynamic PCA, and multiscale PCA—Theoretical anal-

ysis and disturbance detection in the Tennessee Eastman process. AIChE Annual Meeting, 1999, Paper 224g.

[33] G. Chen, T.J. McAvoy, Predictive on-line monitoring of continuous processes, Journal of Process Control 8 (1997) 409–420.

[34] H. Cho, C. Han, Hierarchical plant-wide monitoring and triangular representation based diagnosis, Proc. of the IFAC Online Fault Detection and Supervision in the Chemical Process Industries, Piscataway, NJ, IEEE Press, 1998, pp. 29–34.

[35] C. Georgakis, B. Steadman, V. Liotta, Decentralized PCA charts for performance assessment of plant-wide control structures, Proc. of the 13th IFAC World Congress, Piscataway, NJ, IEEE Press, 1996, pp. 97–101.

[36] J. Gertler, W. Li, Y. Huang, T. McAvoy, Isolation enhanced principal component analysis, AIChE Journal 45 (1999) 323–334.

[37] M. Kano, K. Nagao, S. Hasebe, I. Hashimoto, H. Ohno, R. Strauss, B. Bakshi, Comparison of statistical process monitoring methods: application to the Eastman challenge problem, Computers & Chemical Engineering 24 (2000) 755–760.

[38] D.M. Himes, R.H. Storer, C. Georgakis, Determination of the number of principal components for disturbance detection and isolation, Proc. of the American Control Conf., Piscataway, NJ, IEEE Press, 1994, pp. 1279–1283.

[39] W.E. Larimore, D.E. Seborg, Short Course: Process Monitoring and Identification of Dynamic Systems Using Statistical Techniques, Los Angeles, 1997.

[40] W. Lin, Y. Qian, X. Li, Nonlinear dynamic principal component analysis for on-line process monitoring and diagnosis, Computers & Chemical Engineering 24 (2000) 423–429.

[41] P.R. Lyman, C. Georgakis, Plant-wide control of the Tennessee Eastman problem, Computers & Chemical Engineering 19 (1995) 321–331.